



**HAL**  
open science

## Implementation and validation of a second-moment RANS turbulence model in OpenFOAM ®

Juan P Saldía, Sergio Elaskar, Luis F Gutiérrez Marcantoni, Pascal Bruel

### ► To cite this version:

Juan P Saldía, Sergio Elaskar, Luis F Gutiérrez Marcantoni, Pascal Bruel. Implementation and validation of a second-moment RANS turbulence model in OpenFOAM ®. MECOM 2021 - 37° Congreso Argentino de Mecánica Computacional, Nov 2021, Resistencia, Argentina. hal-03536915

**HAL Id: hal-03536915**

**<https://inria.hal.science/hal-03536915>**

Submitted on 20 Jan 2022

**HAL** is a multi-disciplinary open access archive for the deposit and dissemination of scientific research documents, whether they are published or not. The documents may come from teaching and research institutions in France or abroad, or from public or private research centers.

L'archive ouverte pluridisciplinaire **HAL**, est destinée au dépôt et à la diffusion de documents scientifiques de niveau recherche, publiés ou non, émanant des établissements d'enseignement et de recherche français ou étrangers, des laboratoires publics ou privés.

# Implementation and validation of a second-moment RANS turbulence model in OpenFOAM®

J. P. Saldía <sup>1</sup>, S. Elaskar <sup>1,2</sup>, L. F. Gutiérrez Marcantoni <sup>1,3</sup> and P. Bruel <sup>4</sup>

<sup>1</sup>Departamento de Aeronáutica  
Facultad de Ciencias Exactas, Físicas y Naturales  
Universidad Nacional de Córdoba

<sup>2</sup>Instituto de Estudios Avanzados en Ingeniería y Tecnología UNC/CONICET

<sup>3</sup>Universidad Católica de Córdoba, Facultad de Ingeniería

<sup>4</sup>CNRS - Université de Pau et des Pays de l'Adour - LMAP - Inria CAGIRE Team, France

MECOM 2021  
XXXVII Congreso Argentino de Mecánica Computacional 1 a 5 de Noviembre de 2021  
Resistencia, Chaco, Argentina

## Background

- The no-slip condition at solid interfaces, creates a layered structure for a near-wall turbulent flow, where in the immediate vicinity called viscous sublayer, viscous effects on turbulence cannot be neglected.
- Moreover, the impermeability condition introduces a non-viscous in nature damping, that particularly dampens wall-normal velocity fluctuations.
- This *wall-blocking* effect along with the consequent reflection of pressure fluctuations in the wall, is also felt outside the viscous layer, in the fully turbulent wall region.
- The modeling of these effects it is important for overcoming deficiencies in nonequilibrium flows scenarios, primarily in strong pressure gradients, impinging flows, separation, reattachment, etc. are present.

## Background

- Simple models of near-wall turbulence usually resort to damping functions that depends on the local turbulence Reynolds number and the wall distance that are not well suited to incorporate turbulence anisotropy effects.
- In the context of an eddy viscosity RANS model Durbin (1991) noted that kinematic constraints due to blocking can be introduced through an elliptic model of pressure-velocity fluctuations.
- In this model a separate transport equation was solved for a scalar surrogate of wall-normal velocity fluctuations (designated  $v^2$ ), in conjunction with an *elliptic relaxation* parameter  $f$ , that has become known since as the  $v^2 - f$  model.
- In Durbin (1993) the elliptic relaxation concept is applied, but now in the context of a full second-moment closure. In this latter method, the elliptic relaxation has a tensorial character, which boundary conditions near a solid wall introduce a source of of numerical stiffness and instability.

## Background

- In Manceau and Hanjalić (2002), the authors proposed a model that reduces the tensorial character of Durbin's second-order model to a single scalar elliptic blending variable.
- This model maintains the solid theoretical basis and modeling properties of Durbin's model, while increasing the robustness and ease of implementation and adaptation to industrial CFD codes.

## Second-order RANS equations

- Consider the Reynolds decomposition of the velocity into a mean  $U_i$  and a fluctuating part  $u_i$ .
- The *Reynolds averaged* momentum equation for an incompressible flow of kinematic viscosity  $\nu$  in the absence of external forces reads as:

$$\frac{DU_i}{Dt} = -\frac{\partial P}{\partial x_i} + \frac{\partial}{\partial x_j} \left[ \nu \left( \frac{\partial U_i}{\partial x_j} + \frac{\partial U_j}{\partial x_i} - \overline{u_i u_j} \right) \right]$$

- The Reynolds-stress transport equation reads as:

$$\frac{D\overline{u_i u_j}}{Dt} = P_{ij} + D_{ij}^\nu + D_{ij}^T + \phi_{ij}^* - \epsilon_{ij}$$

- ▶  $P_{ij}$ : turbulent production.
- ▶  $D_{ij}^\nu$ : viscous diffusion.
- ▶  $D_{ij}^T$ : turbulent diffusion by fluctuating velocity.
- ▶  $\phi_{ij}^*$ : fluctuating velocity-pressure gradient correlation.
- ▶  $\epsilon_{ij}$ : turbulence dissipation.

# Elliptic Blending Method (EBM)

- Velocity-pressure gradient correlation, Manceau (2015):

$$\phi_{ij}^* = (1 - \alpha^3)\phi_{ij}^w + \alpha^3\phi_{ij}^h$$

- ▶ Homogeneous term:

$$\begin{aligned}\phi_{ij}^h = & - \left( g_1 + g_1^* \frac{P}{\epsilon} \right) \epsilon b_{ij} + \left( g_3 - g_3^* \sqrt{b_{kl}b_{kl}} \right) k S_{ij} \\ & + g_4 k \left( b_{ik} S_{jk} + b_{jk} S_{ik} - \frac{2}{3} b_{lm} S_{lm} \delta_{ij} \right) \\ & + g_5 k \left( b_{ij} W_{jk} + b_{jk} W_{ik} \right)\end{aligned}$$

where

$$\begin{aligned}b_{ij} &= \frac{\overline{u_i u_j}}{2k} - \frac{1}{3} \delta_{ij} \\ S_{ij} &= \frac{1}{2} \left( \frac{\partial U}{\partial x_j} + \frac{\partial U_j}{\partial x_i} \right), \quad W_{ij} = \frac{1}{2} \left( \frac{\partial U_i}{\partial x_j} - \frac{\partial U_j}{\partial x_i} \right)\end{aligned}$$

- ▶ Wall reflection term:

$$\phi_{ij}^w = -5 \frac{\epsilon}{k} \left[ \overline{u_i u_k} n_j n_k + \overline{u_j u_k} n_i n_k - \frac{1}{2} \overline{u_k u_l} n_k n_l (n_i n_j + \delta_{ij}) \right]$$

- Elliptic relaxation equation:

$$\alpha - L^2 \nabla^2 \alpha = 1$$

- ▶ Approximate wall normal vector:

$$\mathbf{n} = \frac{\nabla \alpha}{\|\nabla \alpha\|}$$

- Turbulent diffusion:

$$D_{ij}^T = \frac{\partial}{\partial x_l} \left( \frac{C_\mu}{\sigma_k} \overline{u_l u_m} T \frac{\partial \overline{u_i u_j}}{\partial x_m} \right)$$

- Time and length scales:

$$T = \max \left( \frac{k}{\epsilon}, C_T \left( \frac{\nu}{\epsilon} \right)^{1/2} \right), \quad L = C_L \max \left( \frac{k^{3/2}}{\epsilon}, C_\eta \frac{\nu^{3/4}}{\epsilon^{1/4}} \right)$$



- Dissipation tensor:

$$\epsilon_{ij} = (1 - \alpha^3) \frac{\overline{u_i u_j}}{k} \epsilon + \frac{2}{3} \alpha^3 \epsilon \delta_{ij}$$

- Turbulence dissipation rate equation:

$$\frac{D\epsilon}{Dt} = \frac{C'_{\epsilon_1} P - C_{\epsilon_2} \epsilon}{T} + \frac{\partial}{\partial x_l} \left( \frac{C_\mu}{\sigma_\epsilon} \overline{u_l u_m T} \frac{\partial \epsilon}{\partial x_m} \right) + \nu \frac{\partial^2 \epsilon}{\partial x_k \partial x_k}$$

where

$$C'_{\epsilon_1} = C_{\epsilon_1} \left[ 1 + A_1 (1 - \alpha^3) \frac{P}{\epsilon} \right]$$

- Model constants:

$$g_1 = 3.4; \quad g_1^* = 1.8; \quad g_3 = 0.8; \quad g_3^* = 1.3; \quad g_4 = 1.25; \quad g_5 = 0.4;$$

$$C_\mu = 0.21; \quad \sigma_k = 1.0; \quad C_T = 6.0; \quad C_L = 0.133; \quad C_\eta = 80.0;$$

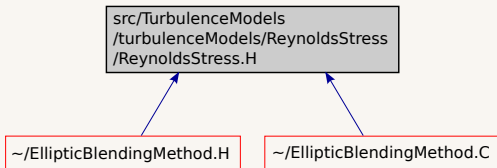
$$C_{\epsilon_1} = 1.44; \quad C_{\epsilon_2} = 1.83; \quad A_1 = 0.065; \quad \sigma_\epsilon = 1.15$$

- Wall boundary conditions:

$$U_i = 0; \quad \overline{u_i u_j} = 0; \quad \epsilon = 2\nu \lim_{y \rightarrow 0} \frac{k}{y^2}; \quad \alpha = 0$$

# Implementation

- Implemented in OpenFOAM<sup>®</sup> v2012 as a class inherited from the ReynoldsStress class:



- We followed guidelines from the implementation that is described by Javadi (2016).
- Code Saturne Archambeau et al. (2004) also provides a publicly available implementation.

## Results

- The implementation has been tested with three cases:
  - ▶ Low Reynolds flow in a plane channel.
  - ▶ Flow over periodic hills.
  - ▶ Flow in an asymmetric diffuser.
- RANS equations are discretized with a collocated second order cell-centered finite volume method and solved through the SIMPLE algorithm.
- Convergent residuals below  $10^{-6}$  were noted in all variables, with the exception of pressure that stalled at  $\approx 10^{-4}$  in most cases.
- With the aim of comparison results with a low Reynolds  $k-\epsilon$  model Launder et al. (1974) were also obtained.

## Plane channel flow

- Fully developed turbulent flow in a plane channel flow at low Reynolds number.
- Results are compared with DNS solutions presented in Kim et al. (1987).
- Reynolds number based on friction velocity corresponds to  $Re_\tau = 180$  and  $Re_\tau = 395$ .
- First wall-normal cell height  $\Delta y^+ \approx 1$ .
- 300 cells in normal direction. One cell in streamwise direction with cyclic boundary conditions.

# Plane channel flow

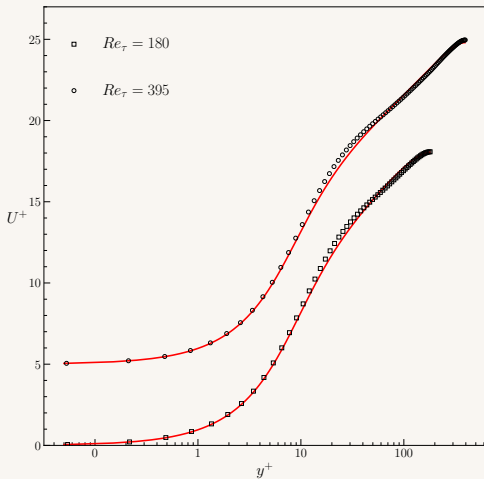
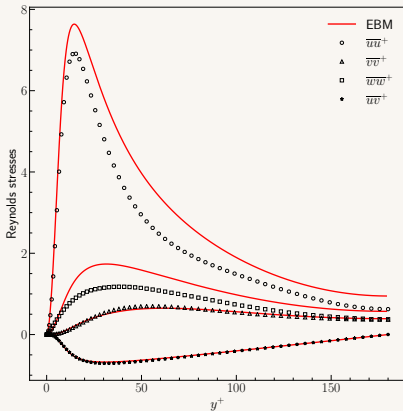
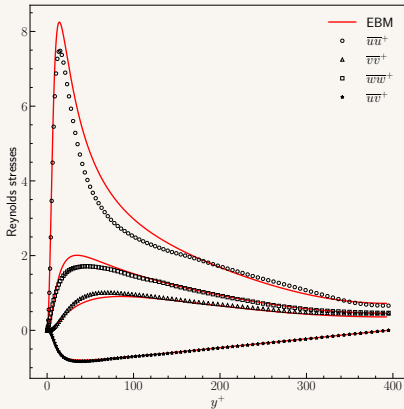


Fig. 1: Velocity profiles for a plane channel flow. Symbols: DNS, Kim et al. (1987); lines: computations with EBM model. Results shifted for clarity.

# Plane channel flow



(a)  $Re_{\tau} = 180$



(b)  $Re_{\tau} = 395$

Fig. 2: Reynolds stresses for a plane channel flow. Symbols: DNS, Kim et al. (1987); lines: computations with EBM model.

## Plane channel flow

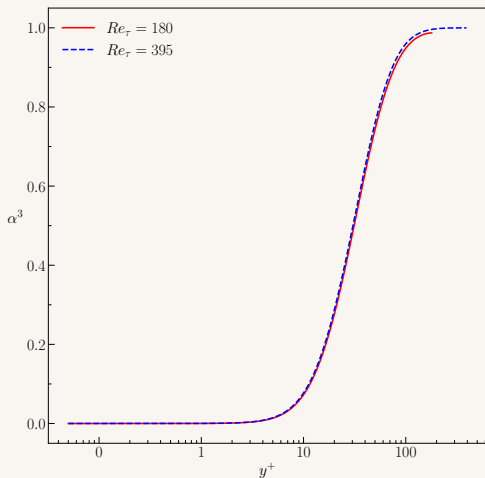


Fig. 3: Elliptic blending function profile for a plane channel flow.

## Flow over periodic hills

- This test corresponds to the 2D turbulent flow over periodic hills numerically investigated by Temmerman et al. (2003)

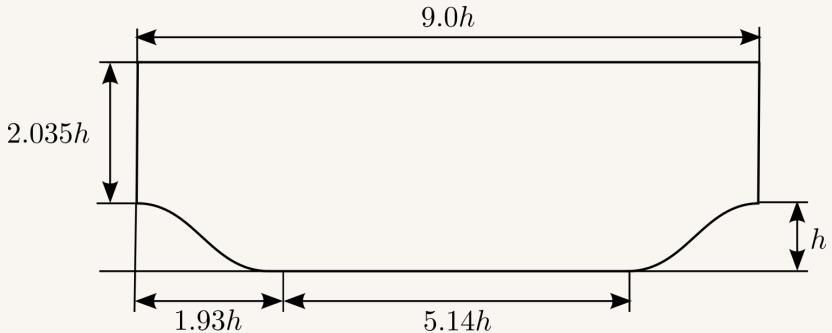


Fig. 4: Periodic hill case description.



## Flow over periodic hills

- Fully developed turbulent flow in a plane channel flow at low Reynolds number.
- Results are compared with LES solutions presented in Temmerman et al. (2003).
- Reynolds number based on bulk velocity and the hill height is  $Re_h = 10595$ .
- Mesh convergence was evaluated in three meshes with increasing level of refinement.
- Coarse:  $100$  (streamwise)  $\times$   $70$  (normal). Semi-coarse:  $100 \times 140$ . Fine:  $200 \times 140$ .
- First wall-normal cell height  $\Delta y^+ \approx 1$  was kept constant in all meshes.

## Flow over periodic hills

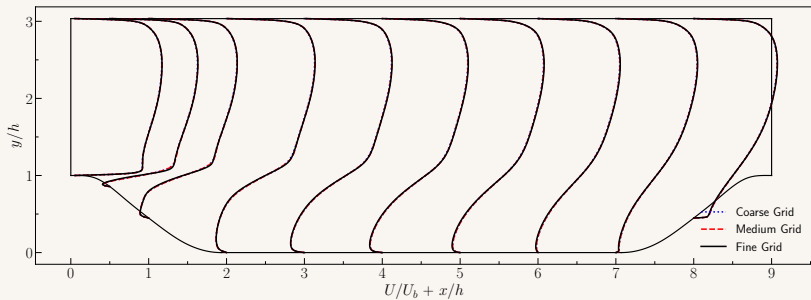
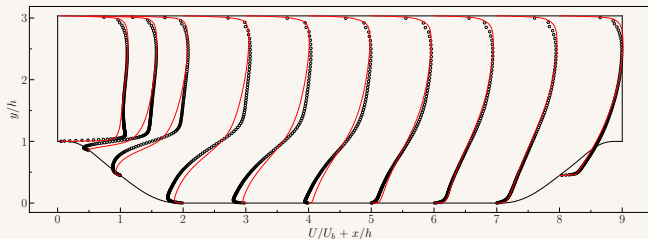
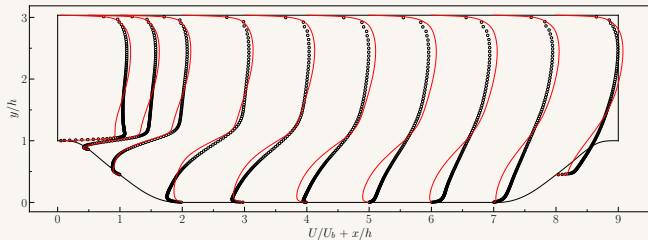


**Fig. 5:** Mesh convergence of flow over periodic hills simulations. Streamwise velocity profiles computed with EBM model.

# Flow over periodic hills



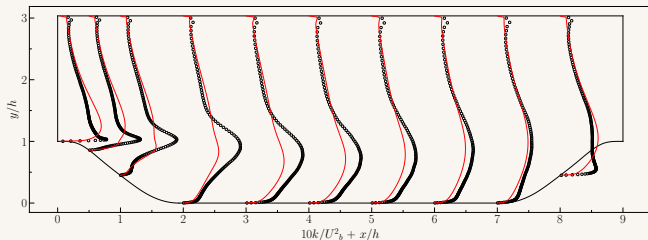
(a) Launder and Sharma low-Reynolds  $k - \epsilon$  model



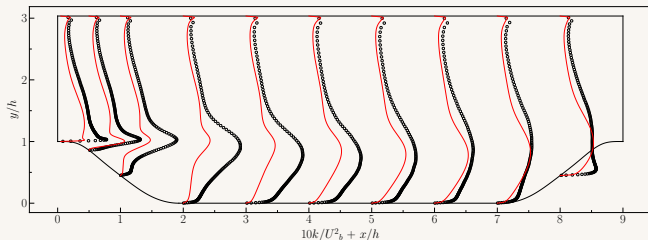
(b) Elliptic blending method

**Fig. 6:** Streamwise velocity profiles for a flow over periodic hills. Symbols: LES Temmerman et al. (2003); lines: computations.

# Flow over periodic hills

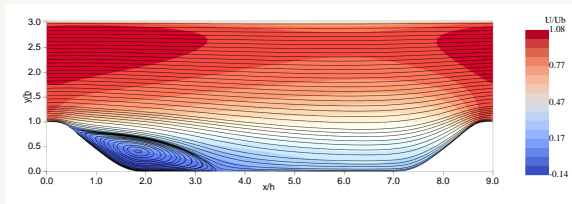


(a) Launder and Sharma low-Reynolds  $k - \epsilon$  model

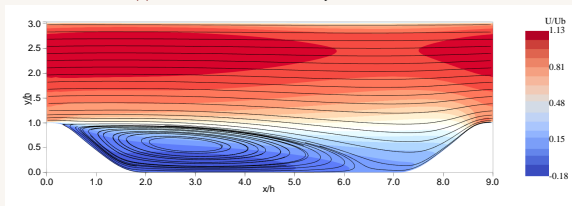


(b) Elliptic blending method

**Fig. 7:** Normal velocity profiles for a flow over periodic hills. Symbols: LES Temmerman et al. (2003); lines: computations.



(a) Launder and Sharma low-Reynolds  $k - \epsilon$  model



(b) Elliptic blending method

**Fig. 8:** Streamline profiles for a flow over periodic hills.

	Separation ( $h$ )	Reattachment ( $h$ )
LES Temmerman et al. (2003)	0.22	4.72
Low Reynolds $k - \epsilon$	0.31	3.51
Elliptic Blending Method	0.26	6.35

## Asymmetric diffuser

- This case corresponds to the separated 2D flow through the axisymmetric diffuser studied experimentally by Buice et al. (2000).

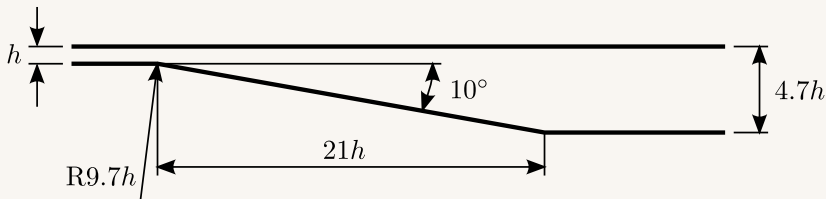
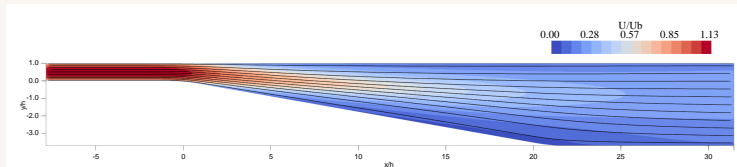


Fig. 9: Asymmetric diffuser geometry

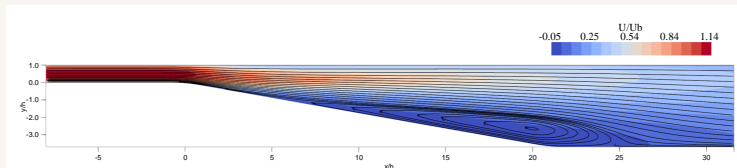
## Flow over periodic hills

- Fully developed turbulent flow in a plane channel flow at low Reynolds number.
- Results are compared with experimental results presented in Buice et al. (2000).
- Reynolds number based on center line velocity and entrance channel height  $h$  is:  $Re_h = 20000$ .
- Mesh convergence was evaluated in three meshes with increasing level of refinement.
- Coarse:  $160$  (streamwise)  $\times$   $140$  (normal). Semi-coarse:  $210 \times 190$ . Fine:  $320 \times 240$ .
- First wall-normal cell height  $\Delta y^+ \approx 0.5$  was kept constant in all meshes.

# Asymmetric diffuser



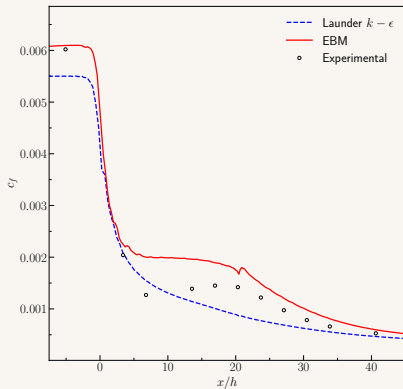
(a) Launder and Sharma low-Reynolds  $k - \epsilon$  model



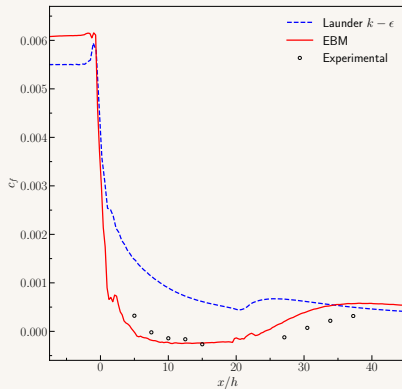
(b) Elliptic blending method

Fig. 10: Streamline profiles for the asymmetric diffuser





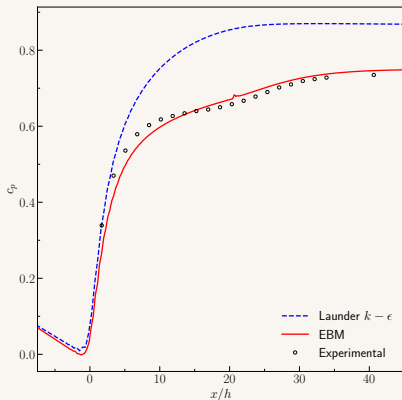
(a) Flat wall



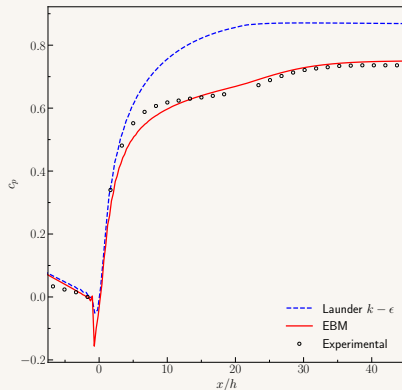
(b) Inclined wall

**Fig. 11:** Friction coefficient for the asymmetric diffuser.  
 Symbols: experiments; lines: computations.

	Separation ( $h$ )	Reattachment ( $h$ )
Experimental Buice et al. (2000)	7.3	29.2
Low reynolds $k - \epsilon$	NA	NA
Elliptic Blending Method	4.56	24.8

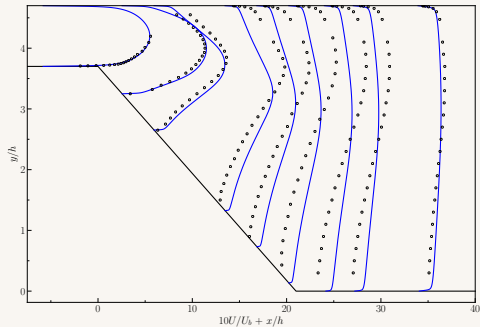


(a) Flat wall

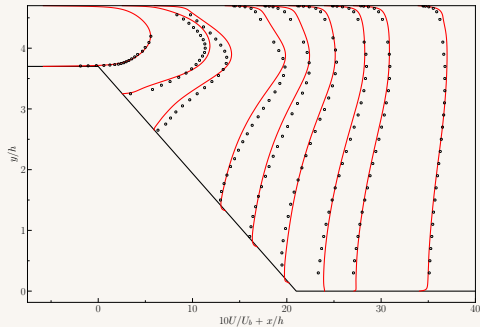


(b) Inclined wall

**Fig. 12:** Pressure coefficient for the asymmetric diffuser.  
 Symbols: experiments; lines: computations.



(a) Launder and Sharma low-Reynolds  $k - \epsilon$  model



(b) Elliptic blending method

**Fig. 13:** Streamwise velocity profiles for the asymmetric diffuser.  
 Symbols: experiments; lines: computations.

## Conclusions

- The implementation and validation of the Elliptic Blending Method in OpenFOAM<sup>®</sup> has been presented.
- Results were compared with high-fidelity numerical solutions corresponding to test cases involving flows with attached and separated boundary layers with streamline curvature effects.
- The performance of the model was also assessed in the separated flow in a 2D asymmetric diffuser where the low-Reynolds  $k - \epsilon$  turbulence model was unable to capture the turbulent separation bubble.
- The implementation is considered satisfactory and as future work further testing in 3D separated flows problems will be considered.

**¡Muchas gracias por su atención!**